Title

Interaction between Prion Protein's Copper-Bound Octarepeat Domain and a Charged C-Terminal Pocket Suggests a Mechanism for N-Terminal Regulation

Journal

Structure, 24(7)

ISSN

1359-0278

Authors

Evans, Eric GB
Pushie, M Jake
Markham, Kate A
et al.

Publication Date

2016-07-01

DOI

10.1016/j.str.2016.04.017

Peer reviewed

Published in final edited form as:

Structure. 2016 July 6; 24(7): 1057–1067. doi:10.1016/j.str.2016.04.017.

Interaction between the Prion Protein's Copper-Bound Octarepeat Domain and a Charged C-terminal Pocket Suggests a Mechanism for N-terminal Regulation

Eric G. B. Evans[1], **M. Jake Pushie**[2], **Kate A. Markham**[1], **Hsiau-Wei Lee**[1], and **Glenn L. Millhauser**[1,*]

[1]Department of Chemistry and Biochemistry, University of California, Santa Cruz, Santa Cruz, CA 95064, USA

[2]Department of Geological Sciences, University of Saskatchewan, Saskatoon, Saskatchewan S7N 5E2, Canada

SUMMARY

Copper plays a critical role in prion protein (PrP) physiology. Cu^{2+} binds with high affinity to the PrP N-terminal octarepeat domain (OR), and intracellular copper promotes PrP expression. The molecular details of copper coordination within the OR are now well characterized. Here we examine how Cu^{2+} influences the interaction between the PrP N-terminal domain and the C-terminal globular domain. Using NMR and copper-nitroxide double electron-electron resonance (DEER) EPR, with molecular dynamics refinement, we localize the position of Cu^{2+} in its high-affinity OR-bound state. Our results reveal an interdomain *cis* interaction that is stabilized by a conserved, negatively charged pocket of the globular domain. Interestingly, this interaction surface overlaps an epitope recognized by the POM1 antibody, the binding of which drives rapid cerebellar degeneration mediated by the PrP N-terminus. The resulting structure suggests that the globular domain regulates the N-terminal domain by binding the Cu^{2+}-occupied OR within a complementary pocket.

Graphical Abstract

*Corresponding Author: glennm@ucsc.edu.

AUTHOR CONTRIBUTIONS

EGBE and GLM designed the experiments; KM expressed several PrP mutants; MJP performed the molecular dynamics calculations; HWL assisted and advised with NMR; EGBE and GLM wrote the manuscript.

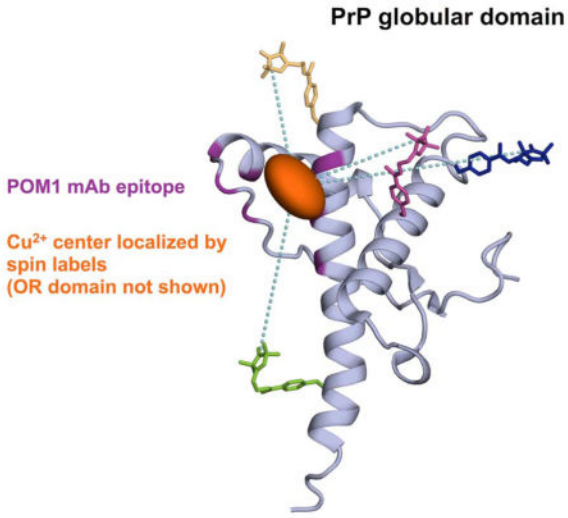

INTRODUCTION

Prion diseases, also known as transmissible spongiform encephalopathies (TSEs), are fatal neurodegenerative diseases of mammals that arise from the conversion of the endogenous cellular prion protein (PrP^C) into an infectious and β-sheet rich form known as PrP scrapie (PrP^{Sc}) (Prusiner, 1982; Soto, 2011). In its mature form, PrP^C is approximately 209 amino acids and consists of a globular C-terminal domain (residues 121–231, human sequence) with three α-helices and one short anti-parallel β-sheet, and a flexible N-terminal domain (residues 23–121) that selectively binds Cu^{2+} and Zn^{2+} (Figure 1) (Riek et al., 1997; Walter et al., 2007). *In vivo*, PrP is attached to the extracellular side of the plasma membrane through a glycophosphatidylinositol (GPI) anchor, and is variably glycosylated at asparagines 181 and 197. Although ubiquitously expressed, PrP^C is enriched at the pre- and postsynaptic membranes of neurons where it is believed to play a critical role in neuronal maintenance, neuroprotection, and metal ion homeostasis (Aguzzi et al., 2008; Herms et al., 1999; Millhauser, 2011; Um et al., 2012).

PrP^C physiology is intimately connected to varying concentrations of the divalent metal ions Cu^{2+} and Zn^{2+}. Cu^{2+} upregulates expression of the *PRNP* gene encoding PrP^C (Armendariz et al., 2004; Varela-Nallar et al., 2006), and both Cu^{2+} and Zn^{2+} stimulate rapid endocytosis and trafficking of PrP in neuronal cells (Brown and Harris, 2003; Hooper et al., 2008; Pauly and Harris, 1998; Perera and Hooper, 2001). PrP has been evolutionarily linked to a subset of the ZIP family of metal ion transporters (Schmitt-Ulms et al., 2009), and regional concentrations of copper, zinc, and iron in the brain correlate with PrP expression levels (Pushie et al., 2011). PrP has also been shown to exert a regulatory effect on a surprisingly large number of cell surface receptors, including ion channels and G protein-coupled receptors, pointing to a multifaceted role in neuronal function (Biasini et al., 2012; Linden et al., 2008). For example, recent work demonstrates that PrP stimulates zinc transport into neuronal cells through interaction with AMPA receptors, a process that requires Zn^{2+} binding directly to PrP^C (Watt et al., 2012). PrP also regulates N-methyl-D-aspartate receptors (NMDAR), protecting against Ca^{2+} overload and cytotoxicity induced by

prolonged glutamate exposure (Stys et al., 2012; You et al., 2012). Importantly, this regulation of NMDAR desensitization by PrP is Cu^{2+}-dependent.

Given the abundance of evidence linking the Cu^{2+} and Zn^{2+} metal ions and PrP function, considerable past effort has aimed to understand the protein's metal-binding properties, particularly with respect to its highest affinity ligand, copper. As a result, the molecular coordination details of PrP Cu^{2+} uptake in the N-terminal octarepeat (OR) domain, and non-OR segments, are now reasonably well understood (Millhauser, 2007). Moreover, analysis of the resulting Cu^{2+} binding features provide insight into the mechanism by which genetic expansion of the OR domain in PrP results in familial prion disease (Stevens et al., 2009). Beyond localized coordination, both Cu^{2+} and Zn^{2+} promote previously unseen long-range tertiary structure in PrP^C (Spevacek et al., 2013; Thakur et al., 2011). In these studies, OR metal binding results in a *cis* interaction between the flexible N-terminal domain and the globular C-terminus. With Zn^{2+} coordination, several point mutations that cause familial prion disease were shown to decrease the apparent strength of this *cis* interaction, suggesting that disruption of interdomain structure may play a role in prion pathogenesis (Spevacek et al., 2013). These results are of particular interest in light of recent monoclonal antibody (mAb) studies showing that the N-terminal domain of PrP^C causes profound neurotoxicity if it is not properly regulated by the globular domain (Sonati et al., 2013). Specifically, mAbs bound to certain regions of the PrP C-terminal domain promote toxic signaling that is executed by the N-terminal domain, resulting in neuronal loss in cerebellar slice preparations. At present, it is unknown how intramolecular N-terminal regulation is achieved and whether or not metal ions are involved. Beyond N-terminal confinement, Cu^{2+} and Zn^{2+} also promote PrP^C α-cleavage, a proteolytic regulatory event that produces the neuroprotective C1 fragment, and is considered to be essential in PrP processing (McDonald et al., 2014). The potential significance of *cis* interactions in PrP^C processing, functional regulation, and prion disease progression is prompting further investigation into the protein's tertiary structure. Thus far, studies examining *cis* interaction have focused on the effects of intrinsic PrP^C charge clusters and physiologic Zn^{2+} ions (Martínez et al., 2015; Spevacek et al., 2013).

Despite the critical role divalent copper plays in PrP^C expression and regulation, little is known about how this relevant, high-affinity metal ion species structures the protein. Here, we investigate the molecular details of interdomain structure in copper-bound PrP using nuclear magnetic resonance (NMR) spectroscopy along with site-directed spin labeling and electron paramagnetic resonance spectroscopy (SDSL-EPR). We employ selective mutagenesis to limit PrP Cu^{2+} coordination to its highest affinity OR binding mode and use ^1H-^{15}N HSQC NMR to map the surface of Cu^{2+}-driven *cis* interaction. We then use double electron-electron resonance (DEER) EPR in frozen solution, along with continuous wave (CW) EPR at room temperature, to directly measure distances between the OR-bound Cu^{2+} ion and genetically incorporated unnatural amino acid spin labels placed at multiple sites in the globular C-terminal domain. Cumulative analysis of Cu^{2+}-nitroxide (Cu-NO) and nitroxide-nitroxide (NO-NO) distances reveal the position of the Cu^{2+} center, and indicate that the Cu^{2+}-bound OR interacts with a highly conserved electronegative pocket of the globular domain defined by surface residues of helices 2 and 3. Our results are supported by constrained molecular dynamics (MD) simulations, which confirm a stable structure driven

primarily by electrostatic interactions. Together, our findings provide a molecular foundation for the role of Cu^{2+} in mediating *cis* interaction in PrP^{C}, and suggest a mechanism by which the globular domain can regulate the N-terminus. Disruption of *cis* interaction, either by mutations that decrease electrostatic interactions or by direct competition with globular domain ligands such as antibodies or PrP^{Sc}, may be a contributing factor in protein dysregulation and prion disease.

RESULTS

Controlling Cu^{2+} Coordination in Full-length PrP

Copper uptake by full-length recombinant PrP is complex and depends critically on the relative concentrations of copper and protein, as well as on solution pH (Aronoff-Spencer et al., 2000; Chattopadhyay et al., 2005; Millhauser, 2007; Whittal et al., 2008). At pH 7.4 the OR binds Cu^{2+} in three distinct coordination modes depending on the relative amount of available copper. At low copper occupancy, a single Cu^{2+} ion is bound by the imidazole side chains of four OR histidine residues in a square planar geometry (Figure 1). This multi-His coordination mode has a net charge of +2 and is commonly referred to as component 3. Reported dissociation constants for component 3 range from ~0.1–10 nM (Nadal et al., 2009; Walter et al., 2006). As the copper-to-protein ratio is increased, OR binding transitions through an intermediate two-His binding mode (component 2) to a high occupancy structure in which each individual repeat of PHGGGWGQ coordinates a single Cu^{2+} ion. This high-occupancy binding mode, known as component 1, coordinates copper through the imidazole nitrogen of histidine, the backbone amide nitrogens from the second and third glycines immediately following the histidine, and the carbonyl oxygen of the third glycine (Burns et al., 2002; Chattopadhyay et al., 2005). PrP also binds copper at two sites just C-terminal to the OR defined by His95 and His110 (mouse sequence) (Burns et al., 2003; Jones et al., 2004; 2005). These sites, variably referred to as the 5^{th} site or non-OR sites, can each bind a single Cu^{2+} ion with nanomolar to sub-nanomolar affinity, placing them roughly equal in affinity to the tightest binding OR mode (component 3) (Nadal et al., 2009; Walter et al., 2009). Finally, the extreme N-terminus of PrP is capable of binding Cu^{2+} through the terminal amino group with a dissociation constant that is roughly equivalent to the single-His (component 1) OR binding mode (Stanyon et al., 2014; Whittal et al., 2008). In total, full-length PrP can bind up to seven equivalents of copper per protein molecule at physiological pH: four in the OR, two in the non-OR sites, and one at the extreme N-terminus.

In order to reduce the complexity of copper binding and facilitate dipolar-based measurements, we adopted two strategies. First, we eliminated non-OR copper binding by mutating residues His95 and His110 to the isostructural amino acid tyrosine. Previous studies of metal-induced *cis* contact in PrP have implicated the OR as the site of interaction (Spevacek et al., 2013; Thakur et al., 2011), and we therefore hypothesized that removal of His95 and His110 would not significantly alter interdomain structure. Indeed, ^{1}H-^{15}N HSQC NMR spectra of wild-type mouse PrP (MoPrP) and MoPrP(H95Y,H110Y) show only minor chemical shift differences confined to residues adjacent in primary sequence to the mutation sites. Secondly, it is well known that Cu^{2+} uptake by PrP is highly sensitive to pH (Aronoff-

Spencer et al., 2000; Whittal et al., 2008). Component 1 binding is strongly inhibited at acidic pH, whereas binding modes that primarily involve imidazole side chain coordination, i.e. component 2 and component 3, are relatively unaffected by pH reductions down to pH ~5. By performing experiments on the MoPrP(H95Y,H110Y) construct at pH 6 with stoichiometric amounts of Cu^{2+}, we are able to selectively probe the highest affinity OR binding mode, component 3, as confirmed by both CW and pulsed EPR measurements (Figure S1).

Cu^{2+}Promotes Interaction at a Specific Surface of the Globular C-terminal Domain

With the ability to direct PrP into a single, high-affinity OR binding mode, we sought to identify the surface of Cu^{2+}-promoted *cis* interaction using NMR spectroscopy. We performed ^{1}H-^{15}N HSQC NMR at 37°C on full-length ^{15}N-labeled MoPrP(H95Y/H110Y) (300 μM) at pH 6.1 in the presence and absence of 1 molar equivalent of Cu^{2+}. Backbone resonance assignments were obtained using a suite of triple-resonance NMR experiments on uniformly ^{15}N,^{13}C-labeled wild type MoPrP(23–230) (see Experimental Procedures). In total, backbone resonances for 135 of 193 (70%) non-proline residues were confirmed under our experimental conditions, including 97 of 108 (90%) globular domain residues (120–230). The addition of Cu^{2+} results in the disappearance of several cross peaks in the HSQC spectrum of MoPrP(H95Y/H110Y), and causes significant broadening (manifested as reduced peak intensities) of many others (Figure 2A and Figure S2). As seen in Figure 2A, the intense cross peak resulting from overlap of the four OR His amide resonances is completely lost upon addition of one equivalent of Cu^{2+}, providing additional evidence that these residues directly contribute to Cu^{2+} coordination. While several resonances are broadened beyond detection, the vast majority of HSQC cross peaks overlay well between the apo and metal-bound spectra, indicating that the overall fold of the protein is not affected by Cu^{2+}-binding (Figure S2).

Cu^{2+}-induced broadening of HSQC resonances were further analyzed by calculating the intensity ratio (I/I_0) for each resonance, where I is the NMR peak intensity in the Cu^{2+}-bound spectrum and I_0 is the peak intensity in the absence of metal ion. Figure 2B shows the calculated intensity ratios for residues 90–230 of MoPrP(H95Y/H110Y). Residues strongly affected by Cu^{2+}-binding (those displaying intensity reductions greater than 1 standard deviation) are colored in red and are primarily localized to three regions: the C-terminal end of the β1-α1 loop extending to the beginning of helix 1, the N-terminal half of helix 2, and the N-terminal half of helix 3. We mapped these residues onto the structure of the MoPrP globular domain (pdb 1xyx) (Gossert et al., 2005), and the results are shown in Figure 2C. Surface plots highlighting the affected residues (Figure 2D) clearly indicate that the Cu^{2+}-mediated *cis* interaction occurs at a specific region of the globular domain defined by the exposed surface of helices 2 and 3, along with the N-terminal portion of helix 1. It is noteworthy that the affected area coincides with a highly conserved, negatively charged electrostatic region of the PrP globular domain (see Discussion).

The NMR peak broadening observed upon Cu^{2+} addition can occur by two primary mechanisms. The first is paramagnetic relaxation enhancement (PRE) of protein nuclei by distance-dependent dipolar interactions with the Cu^{2+} unpaired electron; the second is

chemical exchange in the slow to intermediate regime. PRE from paramagnetic Cu^{2+} typically manifests as peak broadening in the NMR spectrum without significant changes in chemical shift, consistent with what we observe here (Clore and Iwahara, 2009; Donaldson et al., 2001). However, previous NMR studies of PrP also showed HSQC cross peak broadening in the presence of diamagnetic Zn^{2+}, which was interpreted as exchange broadening triggered by N-terminal metal binding (Spevacek et al., 2013). Since PrP does not bind Zn^{2+} under the conditions used in the present study, which were designed to isolate the high-affinity Cu^{2+} binding mode, we cannot readily use Zn^{2+} as a surrogate to determine whether PRE or exchange broadening is the mechanism responsible for the observed Cu^{2+}-induced changes. However, both mechanisms rely on close proximity of the Cu^{2+} center with the globular C-terminal domain.

EPR Spectroscopy Reveals the Location of OR-bound Cu^{2+}

While NMR definitively identifies the region of Cu^{2+}-assisted *cis* interaction on the PrP globular domain, the specific location of the Cu^{2+} ion remains unresolved. We sought to further characterize metal-induced interdomain structure in PrP by utilizing the intrinsically bound OR Cu^{2+} ion as a spin probe. We reasoned that with only a few distance restraints from interelectron dipolar interactions, the approximate location of the Cu^{2+}-occupied OR, relative to the globular domain, could be determined. To facilitate distance measurements between OR Cu^{2+} and globular domain residues, we incorporated stable nitroxide (NO) spin labels at targeted sites in the PrP globular domain using unnatural amino acid spin labeling techniques (Fleissner et al., 2009; Spevacek et al., 2013). Specifically, MoPrP variants were generated on the H95Y/H110Y background in which *p*-acetyl phenylalanine (pAcPhe) was site-specifically introduced into the protein sequence using amber codon suppression (Wang et al., 2003; Young et al., 2010). The resulting keto-functionalized side chains were then selectively reacted to yield the spin-labeled side chain “K1” (Fleissner et al., 2009). This more challenging spin labeling strategy was employed in order to avoid disruption of the native disulfide bond of PrP through introduction of additional cysteines. We chose four surface-exposed sites in the globular domain for spin labeling: Asn180 (α2), Val188 (α2), Thr200 (α3), and Gln222 (α3) (Figure 3A).

Progressive power saturation EPR experiments performed on the four spin-labeled MoPrP constructs show clear, position-dependent changes to the NO saturation profile resulting from dipolar interactions with bound Cu^{2+} (Figure S3), and we therefore aimed to measure Cu-NO distances in these constructs using DEER EPR. DEER has become the gold standard for measuring long-range (~ 2–8 nm) interelectron distances in macromolecules (Jeschke, 2012). Although it is most commonly used to measure pairwise distances between NO spin labels, recent efforts have expanded the DEER technique to include measurements involving paramagnetic metal ions such as Cu^{2+}, Gd^{3+}, Mo^{5+}, and Fe^{3+} (Astashkin et al., 2012; M. Ji et al., 2014; Kaminker et al., 2012). DEER has only recently been employed in the determination of Cu-NO distances, beginning with spin-labeled porphyrin systems (Bode et al., 2008), and progressing to model peptides and copper-binding proteins (Merz et al., 2014; Yang et al., 2010; 2012).

To confirm that accurate Cu-NO distances could be measured with our system, we synthesized a control peptide consisting of the PrP OR-derived sequence HGGGW, followed by a helix-forming poly-alanine based peptide containing a single spin-labeled side chain. Such control peptides have been used extensively by Saxena and co-workers in their development of Cu-NO distance methods (Jun et al., 2006; Yang et al., 2010). DEER at 20K in the presence of excess Cu^{2+} reveals a clear dipolar oscillation and a corresponding narrow distance distribution centered at ~26 Å, in good agreement with molecular models (Figure S4). Next, we performed DEER on the four K1-labeled PrP constructs at pH 6 in the presence of a single equivalent of Cu^{2+}. The background-subtracted time domain DEER traces and the calculated distance distributions are shown in Figure 3B. The time domain data reveal dipolar modulations that are dampened quickly, resulting in broadened distributions in the distance domain. Nevertheless, the data show clearly that the Cu^{2+}-bound OR comes into close contact with the globular domain. Cu-NO distances of highest probability were measured as 17.8, 31.0, 17.6, and 23.1 Å for the N180K1, V188K1, T200K1, and Q222K1 constructs, respectively. The broad distance distributions obtained by DEER indicate that the Cu^{2+}-bound N-terminal domain retains a significant amount of dynamic flexibility, even when docked to the globular domain. These dynamic effects are likely amplified by the known conformational flexibility of the K1 spin label (Fleissner et al., 2009). We note that N180K1 and T200K1 contain additional features at longer distances, but the lack of well-defined modulations in the time-domain data suggest caution in the interpretation of these lower probability features. We therefore constrain our analysis to the maxima of the calculated distributions.

Since the lower limit of interspin distance determination by DEER is ~15 Å, we considered the possibility that shorter Cu-NO distances could exist in our spin-labeled PrP variants. In order to probe this distance regime, we turned to a continuous wave (CW) EPR method developed by Voss and co-workers for measuring distances in the 8–25 Å range between spin-labeled side chains and designed Cu^{2+}-binding sites in proteins (Voss et al., 1995a; 1995b). In this method, dipolar interactions between the spin label and the Cu^{2+} ion are detected as relative amplitude reductions in the field-swept NO EPR spectrum (Leigh, 1970). Notably, this method has proven successful in determining Cu-NO distances in proteins in fluid solution at room temperature (Voss et al., 1998).

We titrated Cu^{2+} into solutions containing each of the four spin-labeled variants of MoPrP(H95Y/H110) (10uM, pH 6.0) and recorded EPR spectra at the NO resonant field (Figure 4). The spectra are consistent with NO side chains in the fast motional regime, with correlation times in the 1–4 ns range, as has been reported for K1-labeled T4 lysozyme (Fleissner et al., 2009). The relative amplitude reductions (I/I_0) for each construct are plotted as a function of added Cu^{2+} in Figure 4B, where I and I_0 are the peak-to-peak amplitudes of the center (m_I=0) line in the Cu^{2+}-bound and Cu^{2+}-free spectra, respectively. Initially, Cu^{2+} produces a steep reduction in NO amplitude that begins to level off after two or three equivalents of titrated metal ion. This is consistent with the first equivalent of Cu^{2+} being taken up by the OR with high affinity as component 3, with subsequent copper binding with lower affinity as component 2 (see also Figure S1). Calculated Cu-NO distances for each spin-labeled construct with one equivalent of Cu^{2+} are shown as red vertical bars superimposed on the DEER distance distributions in Figure 3B. In general, the CW-derived

distances agree remarkably well with the distance probability maxima calculated from the DEER distributions, particularly in the N180K1 and T200K1 PrP variants, where the calculated distances from the two methods are within 1.5 Å. The discrepancy between the two methods is slightly higher for the Q222K1 construct, with the CW method giving a Cu-NO distance that is ~3 Å shorter than the DEER-derived distance. The only spin-labeled PrP variant for which CW and DEER methods do not produce comparable Cu-NO distances is V188K1, where the maximum in the DEER distance distribution is ~10 Å longer than the distance calculated by CW amplitude reduction. It is important to note that the distance calculated by DEER (31 Å) for this construct is well outside of the range accessible by the CW method (~8–25 Å), illustrating the importance of using multiple techniques with different distance range sensitivities, particularly in systems with a broad range of interspin distances.

In order to pinpoint the location of the OR-bound Cu^{2+}-ion relative to the structured domain of PrP, we employed the method of trilateration based on our measured Cu-NO distances. Trilateration using EPR distance measurements has proven successful in determining the location of spin labeled side chains and metal binding sites in proteins (Shah et al., 2014; Yang et al., 2012). We therefore modeled the K1 side chain at positions 180, 188, 200, and 222 onto the published NMR structure of the MoPrP globular domain using the *in silico* spin labeling program mtsslWizard (Hagelueken et al., 2012). Pairwise NO-NO distances were previously determined by DEER for the V188K1/T200K1, V188K1/Q222K1, and T200K1/Q222K1 variants of MoPrP(23–230) (Spevacek et al., 2013) (Table S1). These NO-NO distances were used to select side chain rotamers for V188K1, T200K1, and Q222K1 from the *in silico*-generated rotamer ensemble. Since no experimental evidence was available to guide the rotamer choice for N180K1, the NO position was chosen from the ensemble average of 1,000 allowable spin label conformations generated in mtsslWizard. Trilateration was performed with the program mtsslTrilaterate using the structural coordinates of the four modeled NO electrons and the four experimentally derived Cu-NO distances (Hagelueken et al., 2013).

The results of the Cu^{2+} trilateration, presented in Figure 5, show unequivocally that the Cu^{2+}-ion resides at the exposed surface of helix 3. This calculated region of Cu^{2+} occupancy is in close proximity to the previously identified electronegative pocket on the PrP globular domain, and also coincides with the surface residues affected by Cu^{2+}-binding in the ^{1}H-^{15}N HSQC NMR spectra (Figure 5C). The general region occupied by the Cu^{2+}-ion does not change with variations in Cu-NO distance error input, and is only minimally affected by the choice of spin label conformation used in the trilateration calculations. These results provide strong evidence that the Cu^{2+}-bound OR directly interacts with the exposed surface defined by helix 2, helix 3, and the end of the β1-α1 loop. The proximity of the Cu^{2+} site to acidic residues on helix 3 suggests that electrostatic interactions likely contribute to the *cis* interaction in PrP.

Stability of Interdomain Structure in Cu^{2+}-bound PrP

In order to assess the stability of Cu^{2+}-mediated *cis* interaction, we performed molecular dynamics (MD) simulations with a model construct encompassing the MoPrP globular

domain (pdb 1xyx), the Cu^{2+}-bound OR, and the ~30 residue flexible linker connecting the two. A structural model of the OR with Cu^{2+} bound in the four-coordinate, component 3 binding mode was obtained from previous MD studies (Pushie and Vogel, 2008). Guided by Cu-NO distances from EPR, the copper site of the Cu^{2+}-OR complex was initially placed at the exposed face of helices 2 and 3, and the intervening linker domain residues were constructed manually. After equilibration and energy minimization subject to the DEER restraints, this initial structure was subjected to >500 ns of MD simulation, without external restraints, using the OPLS all-atom force field implemented in GROMACS, supplemented with parameters for the Cu^{2+}-binding environment. Somewhat surprisingly, the interdomain tertiary fold remained intact for the duration of the trajectory in all simulations analyzed, indicating that the *cis* interaction in Cu^{2+}-bound PrP is stable on the time scale of the simulations. A representative snapshot from the MD trajectory, as well as a structural alignment of 50 randomly selected frames spanning ~40 ns of simulation time, is shown in Figure 5D. Analysis of the MD trajectories reveals that the OR-bound Cu^{2+} ion remains closely associated with the exposed surface of helix 3, although its position is closer to the N-terminus of helix 3 than suggested from the DEER-based trilateration (Figure 5D and Movie S1). Analysis of interaction energies from the MD simulations reveals that interdomain association is driven primarily by electrostatic interaction, particularly between Cu^{2+} and Glu199, as well as by hydrophobic contacts between OR residues and surface residues of helix 3. The E199K mutation (E200K in humans), is the most common cause of familial CJD worldwide (Mead, 2006; Minikel et al., 2016), and the participation of this residue in promoting Cu^{2+}-driven *cis* interaction suggests that disruption of interdomain structure may contribute to disease in individuals harboring the E200K mutation.

DISCUSSION

Emerging evidence suggests that tertiary interaction between the flexible N-terminal and globular C-terminal domains of PrP^{C} may serve as a critical regulatory element in PrP physiology. Recent analyses suggest that this *cis* interaction may be mediated by electrostatic charge complementarity between the two domains (Martínez et al., 2015), as well as by metal binding to the N-terminal OR (Spevacek et al., 2013; Thakur et al., 2011). However, little in the way of structural information exists regarding interdomain contact, particularly with regard to the Cu^{2+}-bound protein. Here, we identify the *cis* interaction surface in Cu^{2+}-bound PrP under conditions in which the Cu^{2+} ion is restricted to the high-affinity, multi-His (component 3) binding mode. Given the role of copper in PrP expression and trafficking, coupled with estimates of synaptic Cu^{2+} concentrations and the known sub-nanomolar affinity of component 3, it is likely that this structure represents a relevant *in vivo* PrP state (Walter et al., 2006). Using NMR, we find that Cu^{2+} promotes interaction at a specific surface of the globular domain that largely overlaps with a conserved electronegative pocket at the exposed surface of helices 2 and 3. Furthermore, we reveal the location of the Cu^{2+}-bound OR relative to the structured domain using EPR distance measurements between the intrinsic Cu^{2+}-ion and spin labels placed at select globular domain residues. Our findings are supported by all-atom MD simulations that reveal a tertiary fold stabilized by electrostatic interaction between OR-bound Cu^{2+} and acidic residues of helix 3.

The surface of the PrP globular domain involved in the Cu^{2+}-promoted *cis* interaction observed here overlaps the binding epitopes of several PrP^{C}-specific antibodies that cause acute neurotoxicity (Reimann et al., 2016; Sonati et al., 2013). Sonati *et al.* reported rapid neurotoxicity in mice and cultured cerebellar brain slices with antibody-based ligands that target specific regions of the PrP^{C} globular domain (Sonati et al., 2013). Importantly, the N-terminal domain of PrP is required for the observed toxicity, as deletion of the N-terminal OR, or neutralization with OR-specific antibodies, abolishes the neurotoxic effects of these ligands. Sonati *et al.* propose that the PrP^{C} globular domain acts as a regulator of the N-terminal "effector" domain, and that toxic anti-PrP ligands somehow disrupt this regulatory ability, resulting in deleterious interactions of the N-terminus and subsequent gain-of-function neurotoxicity. This paradigm is supported by studies showing similar neurotoxicity in transgenic mice expressing a GPI-anchored PrP construct lacking the globular domain, although proper cellular localization is impaired in this mutant (Dametto et al., 2015).

The most toxic globular domain antibody studied thus far, POM1, recognizes a non-contiguous epitope consisting of the C-terminal end of the β1-α1 loop, the N-terminal portion of helix 1, and surface exposed residues of helix 3 (Sonati et al., 2013). This epitope lies entirely within the Cu^{2+}-induced *cis* interaction surface we observe here (Figure 5C). Our findings, along with the POM1 toxicity experiments, suggest a physical mechanism whereby the globular domain sequesters the N-terminal domain through the Cu^{2+}-bound OR. This essential regulatory interaction is disrupted by POM1, thus freeing the N-terminal effector domain. Indeed, the crystal structure of MoPrP(120–230) in complex with the $F(ab)_1$ fragment of POM1 shows no structural distortions of the PrP globular domain, again suggesting that the toxic mechanism involves steric inhibition of tertiary or quaternary interactions in full-length PrP (Sonati et al., 2013). It has also been reported that the binding of PrP^{Sc} to PrP^{C} in cell-free conversion assays occurs at or near surface residues of helix 3, as PrP^{Sc} binding was inhibited by an antibody specific for an epitope on helix 3 of PrP^{C} (Horiuchi and Caughey, 1999). This raises the possibility that PrP^{Sc} also inhibits *cis* interaction in PrP^{C} and that this disruption may be an early molecular event in the development of prion disease. This is consistent with the observation that Cu^{2+} and Zn^{2+}, both of which promote interdomain structure, strongly inhibit the *in vitro* amplification of scrapie-induced, protease-resistant PrP (Orem et al., 2006). Furthermore, the neurotoxic pathways induced by POM1 and other globular domain ligands are similar to those observed in prion-infected cultured cerebellar brain slices, suggesting that PrP^{Sc} and the toxic antibodies have similar mechanisms of neurotoxicity (Herrmann et al., 2015).

Electrostatic interaction between positive charges of the N-terminal domain and negative charges of the globular domain surface are known to promote *cis* interaction in PrP (Martínez et al., 2015; Spevacek et al., 2013; Thakur et al., 2011). Here we show that OR-bound Cu^{2+} participates directly in the stabilization of interdomain structure through electrostatic interaction with acidic residues on helix 3. The majority of *PRNP* gene mutations that give rise to human prion disease result in point mutations on helices 2 and 3 and often involve amino acid substitutions that attenuate the overall negative charge of this domain (Shen and H.-F. Ji, 2011). We have shown previously that several disease-associated mutants, including E199K and D177N (mouse sequence), weaken *cis* interaction induced by Zn^{2+} binding (Spevacek et al., 2013), and analysis of MD interaction energies in the present

study predict a similar destabilization of the Cu^{2+}-driven fold. It is therefore plausible that a disruption of metal-mediated *cis* interaction may be a causative factor in certain inherited prion diseases.

The nature of the Cu^{2+}-driven *cis* interaction observed here also suggests new interpretations of prion disease caused by genetic OR expansion and deletion. Genetic insertion of four or more additional octarepeat segments of PHGGGWGQ into the PrP sequence results in early onset prion disease in humans (Mead, 2006). Interestingly, though prion disease has been reported in individuals with three or fewer repeat insertions, these cases typically lack family history, occur later in life, and are incompletely penetrant, suggesting that they may be rare polymorphisms (Beck et al., 2010). This shift in disease phenotype between three and four extra repeats correlates with the copper-binding properties of the PrP OR (Stevens et al., 2009). With four or more additional repeats, the OR can accommodate two Cu^{2+} ions in the multi-His (component 3) binding mode, resulting in persistence of this high-affinity coordination environment even at high concentrations of Cu^{2+} where OR coordination normally shifts toward the single-His (component 1) mode. The simultaneous presence of multiple charged Cu^{2+} complexes in the OR would likely alter normal Cu^{2+}-mediated *cis* interaction with the globular domain. Even if an interdomain structure such as that presented here exists in proteins bearing supernumerary repeats, there would still be long segments of uncomplexed N-terminus, likely Cu^{2+}-bound, capable of transducing a toxic signal either through aberrant cellular interactions or redox activity.

Deletion of one octarepeat segment is a neutral polymorphism in humans; however, deletion of two repeats results in lethal prion disease (Beck et al., 2010; Mead, 2006). This is interesting considering that at least three octarepeat segments are required to bind Cu^{2+} in a component 3-type binding mode (Chattopadhyay et al., 2005). Perhaps the pathogenicity of two-repeat deletions stems from the inability to promote *cis* interaction through multi-His Cu^{2+} coordination, while still retaining enough of the OR to provoke toxic signaling.

In summary, we have provided molecular details of interdomain structure in Cu^{2+}-bound PrP in which Cu^{2+} coordination has been limited to the highest affinity OR binding mode. Both NMR and DEER EPR reveal that the globular domain surface involved in Cu^{2+}-driven *cis* interaction coincides with a well-defined electronegative surface of the PrP globular domain and shares conspicuous overlap with the epitopes of several PrP antibodies known to cause severe neurotoxicity. All-atom MD simulations show that the *cis* interaction is stabilized by electrostatic interaction between the Cu^{2+}-bound OR and acidic residues of helix 3, as well as by multiple hydrophobic interactions between the OR and helix 3. When reconciled with recent antibody experiments, our findings predict that disruption of the interdomain structure observed here may contribute to the observed N-terminal neurotoxicity, and may also be a general molecular mechanism common to several forms of inherited prion disease. This current study is limited to the OR complexed with a single Cu^{2+} ion. However, as demonstrated previously, the OR domain is responsive to varying concentrations of copper, and adopts distinct conformations when challenged with additional copper equivalents. Moreover, there are two additional copper sites between the OR and the globular domain. Future studies exploring how these additional sites, and varying copper concentrations,

affect N-terminal regulation are certain to provide important insights into PrP-mediated neurodegeneration.

EXPERIMENTAL PROCEDURES

NMR

NMR experiments were conducted on a Varian INOVA 600-MHz spectrometer equipped with a ^{1}H, ^{13}C, ^{15}N triple-resonance cryoprobe. ^{1}H-^{15}N resonance assignments were obtained using standard triple-resonance experiments with a 400 μM uniformly ^{13}C,^{15}N-labeled MoPrP(23–230) sample at 25°C. Experiments included HNCO, HN(CA)CO, HNCACB, CBCA(CO)NH, and CC(CO)NH. The assignments were then transferred to the ^{1}H-^{15}N HSQC spectrum at 300 μM and 37°C by following the cross-peaks through concentration and temperature titrations. Resonances were confirmed, and additional resonances were assigned, by recording three-dimensional HNCACB and ^{15}N-NOESY-HSQC spectra at 300 μM and 37°C. Finally, resonance assignments were transferred to the ^{1}H,^{15}N HSQC spectrum of MoPrP (H95Y/H110Y) at 300 μM and 37°C by visual inspection. All NMR spectra were processed with NMRPipe and NMRDraw (Delaglio et al., 1995), and analyzed using CcpNmr Analysis (Vranken et al., 2005).

^{1}H,^{15}N HSQC spectra were recorded for MoPrP (H95Y/H110Y) constructs (300 μM) at 37°C both in the absence of metal ions and in the presence of 300 μM $CuCl_2$, and the HSQC peak intensities were determined using CcpNmr Analysis. Intensity ratios were analyzed using Kaleidagraph (Synergy Software) and residues with intensity reductions greater the one standard deviation of the mean were considered significantly perturbed.

EPR

CW EPR spectra were recorded at room temperature on a Bruker EMX spectrometer at ~9.5 GHz with a Bruker 4122SHQE resonator. Spectra were recorded at 298K with a microwave power of 20mW, a modulation amplitude of 1 Gauss, and a sweep width of 150 Gauss. Spectra were baseline subtracted and corrected using a LabVIEW (National Instruments) program written in-house. For Cu^{2+} titrations, each data point is the average of three separate samples. Signal intensities were measured as the peak-to-peak amplitude of the center (m_I=0) resonance of the nitroxide spectrum.

Dipolar interaction coefficients (C) were calculated from the normalized amplitude (I/I_0) in the presence of 1 equivalent Cu^{2+} using the following equation, empirically derived by Voss *et al.* (Voss et al., 1995b).

$$\frac{I}{I_0}=\frac{(I/I_0)_0-(I/I_0)_\infty}{1+\left(\frac{C/\Delta H_0}{k_{1/2}}\right)^p}+\left(\frac{I}{I_0}\right)_\infty$$

For a spin label undergoing rapid isotropic motion, ΔH_0 is the peak-to-peak line width of the nitroxide, $(I/I_0)_0$ = 1.1, $(I/I_0)_\infty$ = 0.0435, $k_{1/2}$ = 0.739, and p = 0.861 (Voss et al., 1995b).

The Cu^{2+}-NO distance, r, was then calculated for each spin-labeled PrP variant using the formula

$$C=\frac{g\beta_e\mu^2\tau}{\hbar r^6},$$

where g is the isotropic g-factor of the nitroxide, β_e is the Bohr magneton, μ is the Cu^{2+} magnetic moment, $\hbar$ is the reduced Planck constant, and $\tau = T_{1e}(Cu^{2+}) \approx 3\times10^{-9}$ s.

DEER EPR experiments were performed at 20 K on a Bruker E580 pulsed X-band spectrometer at ~9.7 GHz with a Bruker MD-5 dielectric resonator. The 4-pulse DEER experiment was employed, consisting of the pulse sequence $(\pi/2)_{obs} - \tau_1 - (\pi)_{obs} - T - (\pi)_{pump} - \tau_2 - (\pi)_{obs} - \tau_2 -$ (echo). The observer pulse frequency was set to the center of the resonator mode and the magnetic field was adjusted to correspond to the maximum of the Cu^{2+} signal in the echo-detected field-swept spectrum. The pump pulse was chosen at a frequency 210–277 MHz lower than the observer frequency and corresponded to the maximum of the nitroxide spectrum. Observer and pump π pulses were 16 and 12 ns, respectively, and a 2-step phase cycle was employed on the observer $\pi/2$ pulse. Proton modulations were suppressed by adding spectra recorded at 8 different values of τ_1 beginning at 160 ns and incrementing by 8 ns intervals. Spectra were signal averaged for 8–28 hr, depending on the sample concentration, and data were analyzed in LabVIEW with the LongDistances program (C. Altenbach, available at http://www.biochemistry.ucla.edu/biochem/Faculty/Hubbell/).

Trilateration

K1 spin-labeled side chains were modeled onto the NMR structure of MoPrP(120–230, pdb 1xyx) using mtslWizard (Hagelueken et al., 2012). For labels at positions V188, T200, and Q222, spin-label conformers were chosen from the rotameric ensemble based on the experimentally derived interspin distances for V188K1/T200K1, V188K1/Q222K1, and T200K1/Q222K1 previously reported for full-length MoPrP (Spevacek et al., 2013). Specifically, rotamers were chosen that gave internitroxide distances within 2 Å of the DEER-derived distances. The K1 rotamer at the N180 position was chosen as the average of 1,000 allowable label conformations, avoiding hard sphere overlap with the protein. The coordinates of the NO electron from each K1 label was used in combination with Cu^{2+}-NO distances from DEER measurements to locate the Cu^{2+} ion in three-dimensional space using the program mtslTrilaterate (Hagelueken et al., 2013). All molecular analysis and graphical representations were performed in PyMOL (DeLano, 2010).

Molecular Dynamics

Molecular dynamics simulations were performed with GROMACS 4.5 using the OPLS-AA force field modified to include parameterization of the square planar Cu^{2+} center (Jorgensen et al., 1996; Pronk et al., 2013; Pushie and Vogel, 2008). The initial model was constructed from the MoPrP globular domain NMR structure (residues 120–230, pdb 1xyx) extended to include the Cu^{2+}-bound OR and the intervening linker (residues 59–119). Additional

refinements to the component 3 coordination structure were included from recent EXAFS and DFT calculations (Pushie et al., 2014). The initial structure was subjected to steepest-decent energy minimization with interdomain arrangement restrained by the experimental distances obtained with DEER EPR. The resulting structures were then simulated with the modified OPLS force field in explicit solvent using the SPC water model as described previously (Berendsen et al., 1984; Pushie and Vogel, 2008).

Supplementary Material

Refer to Web version on PubMed Central for supplementary material.

Acknowledgments

This work was funded by a grant from the National Institutes of Health (GM065790 awarded to G.L.M.). The authors thank Ms. Aracely Acevedo for assistance with protein preparation. Drs. Wayne Hubbell and Mark Fleissner (UCLA) are gratefully acknowledged for their assistance with technologies for incorporation of the K1 label.

References

Aguzzi A, Baumann F, Bremer J. The prion's elusive reason for being. Annu Rev Neurosci. 2008; 31:439–477. [PubMed: 18558863]

Armendariz AD, Gonzalez M, Loguinov AV, Vulpe CD. Gene expression profiling in chronic copper overload reveals upregulation of Prnp and App. Physiol Genomics. 2004; 20:45–54. [PubMed: 15467011]

Aronoff-Spencer E, Burns CS, Avdievich NI, Gerfen GJ, Peisach J, Antholine WE, Ball HL, Cohen FE, Prusiner SB, Millhauser GL. Identification of the Cu2+ binding sites in the N-terminal domain of the prion protein by EPR and CD spectroscopy. Biochemistry. 2000; 39:13760–13771. [PubMed: 11076515]

Astashkin AV, Rajapakshe A, Cornelison MJ, Johnson-Winters K, Enemark JH. Determination of the distance between the Mo(V) and Fe(III) heme centers of wild type human sulfite oxidase by pulsed EPR spectroscopy. J Phys Chem B. 2012; 116:1942–1950. [PubMed: 22229742]

Beck JA, Poulter M, Campbell TA, Adamson G, Uphill JB, Guerreiro R, Jackson GS, Stevens JC, Manji H, Collinge J, Mead S. PRNP allelic series from 19 years of prion protein gene sequencing at the MRC Prion Unit. Hum Mutat. 2010; 31:E1551–E1563. [PubMed: 20583301]

Berendsen HJC, Postma JPM, van Gunsteren WF, DiNola A, Haak JR. Molecular dynamics with coupling to an external bath. J Chem Phys. 1984; 81:3684–3690.

Biasini E, Turnbaugh JA, Unterberger U, Harris DA. Prion protein at the crossroads of physiology and disease. Trends Neurosci. 2012; 35:92–103. [PubMed: 22137337]

Bode BE, Plackmeyer J, Prisner TF, Schiemann O. PELDOR measurements on a nitroxide-labeled Cu(II) porphyrin: orientation selection, spin-density distribution, and conformational flexibility. J Phys Chem A. 2008; 112:5064–5073. [PubMed: 18491846]

Brown LR, Harris DA. Copper and zinc cause delivery of the prion protein from the plasma membrane to a subset of early endosomes and the Golgi. J Neurochem. 2003; 87:353–363. [PubMed: 14511113]

Burns CS, Aronoff-Spencer E, Dunham CM, Lario P, Avdievich NI, Antholine WE, Olmstead MM, Vrielink A, Gerfen GJ, Peisach J, Scott WG, Millhauser GL. Molecular features of the copper binding sites in the octarepeat domain of the prion protein. Biochemistry. 2002; 41:3991–4001. [PubMed: 11900542]

Burns CS, Aronoff-Spencer E, Legname G, Prusiner SB, Antholine WE, Gerfen GJ, Peisach J, Millhauser GL. Copper coordination in the full-length, recombinant prion protein. Biochemistry. 2003; 42:6794–6803. [PubMed: 12779334]

Chattopadhyay M, Walter ED, Newell DJ, Jackson PJ, Aronoff-Spencer E, Peisach J, Gerfen GJ, Bennett B, Antholine WE, Millhauser GL. The octarepeat domain of the prion protein binds Cu(II) with three distinct coordination modes at pH 7.4. J Am Chem Soc. 2005; 127:12647–12656. [PubMed: 16144413]

Clore GM, Iwahara J. Theory, practice, and applications of paramagnetic relaxation enhancement for the characterization of transient low-population states of biological macromolecules and their complexes. Chem Rev. 2009; 109:4108–4139. [PubMed: 19522502]

Dametto P, Lakkaraju AKK, Bridel C, Villiger L, O'Connor T, Herrmann US, Pelczar P, Rülicke T, McHugh D, Adili A, Aguzzi A. Neurodegeneration and Unfolded-Protein Response in Mice Expressing a Membrane-Tethered Flexible Tail of PrP. PLoS ONE. 2015; 10:e0117412. [PubMed: 25658480]

Delaglio F, Grzesiek S, Vuister GW, Zhu G, Pfeifer J, Bax A. NMRPipe: a multidimensional spectral processing system based on UNIX pipes. J Biomol NMR. 1995; 6:277–293. [PubMed: 8520220]

DeLano, WL. The PyMOL Molecular Graphics System, Ver. 1.3. Schrödinger; Portland, OR: 2010.

Donaldson LW, Skrynnikov NR, Choy WY, Muhandiram DR, Sarkar B, Forman-Kay JD, Kay LE. Structural characterization of proteins with an attached ATCUN motif by paramagnetic relaxation enhancement NMR spectroscopy. J Am Chem Soc. 2001; 123:9843–9847. [PubMed: 11583547]

Fleissner MR, Brustad EM, Kálai T, Altenbach C, Cascio D, Peters FB, Hideg K, Peuker S, Schultz PG, Hubbell WL. Site-directed spin labeling of a genetically encoded unnatural amino acid. Proc Natl Acad Sci USA. 2009; 106:21637–21642. [PubMed: 19995976]

Gossert AD, Bonjour S, Lysek DA, Fiorito F, Wüthrich K. Prion protein NMR structures of elk and of mouse/elk hybrids. Proc Natl Acad Sci USA. 2005; 102:646–650. [PubMed: 15647363]

Hagelueken G, Abdullin D, Ward R, Schiemann O. mtsslSuite: In silico spin labelling, trilateration and distance-constrained rigid body docking in PyMOL. Mol Phys. 2013; 111:2757–2766. [PubMed: 24954955]

Hagelueken G, Ward R, Naismith JH, Schiemann O. MtsslWizard: In silico spin-labeling and generation of distance distributions in PyMOL. Appl Magn Reson. 2012; 42:377–391. [PubMed: 22448103]

Herms J, Tings T, Gall S, Madlung A, Giese A, Siebert H, Schürmann P, Windl O, Brose N, Kretzschmar H. Evidence of presynaptic location and function of the prion protein. J Neurosci. 1999; 19:8866–8875. [PubMed: 10516306]

Herrmann US, Sonati T, Falsig J, Reimann RR, Dametto P, O'Connor T, Li B, Lau A, Hornemann S, Sorce S, Wagner U, Sanoudou D, Aguzzi A. Prion Infections and Anti-PrP Antibodies Trigger Converging Neurotoxic Pathways. PLoS Pathog. 2015; 11:e1004662. [PubMed: 25710374]

Hooper NM, Taylor DR, Watt NT. Mechanism of the metal-mediated endocytosis of the prion protein. Biochem Soc Trans. 2008; 36:1272–1276. [PubMed: 19021539]

Horiuchi M, Caughey B. Specific binding of normal prion protein to the scrapie form via a localized domain initiates its conversion to the protease-resistant state. EMBO J. 1999; 18:3193–3203. [PubMed: 10369660]

Jeschke G. DEER Distance Measurements on Proteins. Annu Rev Phys Chem. 2012; 63:419–446. [PubMed: 22404592]

Ji M, Ruthstein S, Saxena S. Paramagnetic metal ions in pulsed ESR distance distribution measurements. Acc Chem Res. 2014; 47:688–695. [PubMed: 24289139]

Jones CE, Abdelraheim SR, Brown DR, Viles JH. Preferential Cu2+ coordination by His96 and His111 induces beta-sheet formation in the unstructured amyloidogenic region of the prion protein. J Biol Chem. 2004; 279:32018–32027. [PubMed: 15145944]

Jones CE, Klewpatinond M, Abdelraheim SR, Brown DR, Viles JH. Probing copper2+ binding to the prion protein using diamagnetic nickel2+ and 1H NMR: the unstructured N terminus facilitates the coordination of six copper2+ ions at physiological concentrations. J Mol Biol. 2005; 346:1393–1407. [PubMed: 15713489]

Jorgensen WL, Max LDS, Tirado-Rives J. Development and testing of the OPLS all-atom force field on conformational energetics and properties of organic liquids. J Am Chem Soc. 1996; 118:11225–11236.

Jun S, Becker JS, Yonkunas M, Coalson R, Saxena S. Unfolding of alanine-based peptides using electron spin resonance distance measurements. Biochemistry. 2006; 45:11666–11673. [PubMed: 16981726]

Kaminker I, Yagi H, Huber T, Feintuch A, Otting G, Goldfarb D. Spectroscopic selection of distance measurements in a protein dimer with mixed nitroxide and Gd3+ spin labels. Phys Chem Chem Phys. 2012; 14:4355–4358. [PubMed: 22362220]

Leigh JS. ESR Rigid-Lattice Line Shape in a System of Two Interacting Spins. J Chem Phys. 1970; 52:2608–2612.

Linden R, Martins VR, Prado MAM, Cammarota M, Izquierdo I, Brentani RR. Physiology of the Prion Protein. Physiol Rev. 2008; 88:673–728. [PubMed: 18391177]

Martínez J, Sánchez R, Castellanos M, Makarava N, Aguzzi A, Baskakov IV, Gasset M. PrP charge structure encodes interdomain interactions. Sci Rep. 2015; 5:13623. [PubMed: 26323476]

McDonald AJ, Dibble JP, Evans EGB, Millhauser GL. A New Paradigm for Enzymatic Control of α-Cleavage and β-Cleavage of the Prion Protein. J Biol Chem. 2014; 289:803–813. [PubMed: 24247244]

Mead S. Prion disease genetics. Eur J Hum Genet. 2006; 14:273–281. [PubMed: 16391566]

Merz GE, Borbat PP, Pratt AJ, Getzoff ED, Freed JH, Crane BR. Copper-based pulsed dipolar ESR spectroscopy as a probe of protein conformation linked to disease states. Biophys J. 2014; 107:1669–1674. [PubMed: 25296320]

Millhauser GL. Copper and Prion Protein Function: A Brief Review of Emerging Theories of Neuroprotection. RSC Drug Discovery. 2011

Millhauser GL. Copper and the prion protein: methods, structures, function, and disease. Annu Rev Phys Chem. 2007; 58:299–320. [PubMed: 17076634]

Minikel EV, Vallabh SM, Lek M, Estrada K, Samocha KE, Sathirapongsasuti JF, McLean CY, Tung JY, Yu LPC, Gambetti P, Blevins J, Zhang S, Cohen Y, Chen W, Yamada M, Hamaguchi T, Sanjo N, Mizusawa H, Nakamura Y, Kitamoto T, Collins SJ, Boyd A, Will RG, Knight R, Ponto C, Zerr I, Kraus TFJ, Eigenbrod S, Giese A, Calero M, de Pedro-Cuesta J, Haïk S, Laplanche JL, Bouaziz-Amar E, Brandel JP, Capellari S, Parchi P, Poleggi A, Ladogana A, O'Donnell-Luria AH, Karczewski KJ, Marshall JL, Boehnke M, Laakso M, Mohlke KL, Kähler A, Chambert K, McCarroll S, Sullivan PF, Hultman CM, Purcell SM, Sklar P, van der Lee SJ, Rozemuller A, Jansen C, Hofman A, Kraaij R, van Rooij JGJ, Ikram MA, Uitterlinden AG, van Duijn CM, Daly MJ, MacArthur DG. Exome Aggregation Consortium (ExAC). Quantifying prion disease penetrance using large population control cohorts. Sci Transl Med. 2016; 8:322ra9.

Nadal RC, Davies P, Brown DR, Viles JH. Evaluation of copper2+ affinities for the prion protein. Biochemistry. 2009; 48:8929–8931. [PubMed: 19697960]

Orem NR, Geoghegan JC, Deleault NR, Kascsak R, Supattapone S. Copper (II) ions potently inhibit purified PrPres amplification. J Neurochem. 2006; 96:1409–1415. [PubMed: 16417569]

Pauly PC, Harris DA. Copper stimulates endocytosis of the prion protein. J Biol Chem. 1998; 273:33107–33110. [PubMed: 9837873]

Perera WS, Hooper NM. Ablation of the metal ion-induced endocytosis of the prion protein by disease-associated mutation of the octarepeat region. Curr Biol. 2001; 11:519–523. [PubMed: 11413003]

Pronk S, Páll S, Schulz R, Larsson P, Bjelkmar P, Apostolov R, Shirts MR, Smith JC, Kasson PM, van der Spoel D, Hess B, Lindahl E. GROMACS 4.5: a high-throughput and highly parallel open source molecular simulation toolkit. Bioinformatics. 2013; 29:845–854. [PubMed: 23407358]

Prusiner SB. Novel proteinaceous infectious particles cause scrapie. Science. 1982; 216:136–144. [PubMed: 6801762]

Pushie MJ, Nienaber KH, Mcdonald A, Millhauser GL, George GN. Combined EXAFS and DFT structure calculations provide structural insights into the 1:1 multi-histidine complexes of Cu(II), Cu(I), and Zn(II) with the tandem octarepeats of the mammalian prion protein. Chem Eur J. 2014; 20:9770–9783. [PubMed: 25042361]

Pushie MJ, Pickering IJ, Martin GR, Tsutsui S, Jirik FR, George GN. Prion protein expression level alters regional copper, iron and zinc content in the mouse brain. Metallomics. 2011; 3:206–214. [PubMed: 21264406]

Pushie MJ, Vogel HJ. Modeling by assembly and molecular dynamics simulations of the low Cu2+ occupancy form of the mammalian prion protein octarepeat region: gaining insight into Cu2+-mediated beta-cleavage. Biophys J. 2008; 95:5084–5091. [PubMed: 18790846]

Reimann RR, Sonati T, Hornemann S, Herrmann US, Arand M, Hawke S, Aguzzi A. Differential Toxicity of Antibodies to the Prion Protein. PLoS Pathog. 2016; 12:e1005401. [PubMed: 26821311]

Riek R, Hornemann S, Wider G, Glockshuber R, Wüthrich K. NMR characterization of the full-length recombinant murine prion protein, mPrP(23–231). FEBS Lett. 1997; 413:282–288. [PubMed: 9280298]

Schmitt-Ulms G, Ehsani S, Watts JC, Westaway D, Wille H. Evolutionary descent of prion genes from the ZIP family of metal ion transporters. PLoS ONE. 2009; 4:e7208. [PubMed: 19784368]

Shah C, Hegde BG, Morén B, Behrmann E, Mielke T, Moenke G, Spahn CMT, Lundmark R, Daumke O, Langen R. Structural Insights into Membrane Interaction and Caveolar Targeting of Dynamin-like EHD2. Structure. 2014; 22:409–420. [PubMed: 24508342]

Shen L, Ji HF. Mutation directional selection sheds light on prion pathogenesis. Biochem Biophys Res Commun. 2011; 410:159–163. [PubMed: 21679685]

Sonati T, Reimann RR, Falsig J, Baral PK, O'Connor T, Hornemann S, Yaganoglu S, Li B, Herrmann US, Wieland B, Swayampakula M, Rahman MH, Das D, Kav N, Riek R, Liberski PP, James MNG, Aguzzi A. The toxicity of antiprion antibodies is mediated by the flexible tail of the prion protein. Nature. 2013; 501:102–106. [PubMed: 23903654]

Soto C. Prion hypothesis: the end of the controversy? Trends Biochem Sci. 2011; 36:151–158. [PubMed: 21130657]

Spevacek AR, Evans EGB, Miller JL, Meyer HC, Pelton JG, Millhauser GL. Zinc drives a tertiary fold in the prion protein with familial disease mutation sites at the interface. Structure. 2013; 21:236–246. [PubMed: 23290724]

Stanyon HF, Patel K, Begum N, Viles JH. Copper(II) sequentially loads onto the N-terminal amino group of the cellular prion protein before the individual octarepeats. Biochemistry. 2014; 53:3934–3999. [PubMed: 24878028]

Stevens DJ, Walter ED, Rodríguez A, Draper D, Davies P, Brown DR, Millhauser GL. Early onset prion disease from octarepeat expansion correlates with copper binding properties. PLoS Pathog. 2009; 5:e1000390. [PubMed: 19381258]

Stys PK, You H, Zamponi GW. Copper-dependent regulation of NMDA receptors by cellular prion protein: implications for neurodegenerative disorders. J Physiol. 2012; 590:1357–1368. [PubMed: 22310309]

Thakur AK, Srivastava AK, Srinivas V, Chary KVR, Rao CM. Copper alters aggregation behavior of prion protein and induces novel interactions between its N- and C-terminal regions. J Biol Chem. 2011; 286:38533–38545. [PubMed: 21900252]

Um JW, Nygaard HB, Heiss JK, Kostylev MA, Stagi M, Vortmeyer A, Wisniewski T, Gunther EC, Strittmatter SM. Alzheimer amyloid-β oligomer bound to postsynaptic prion protein activates Fyn to impair neurons. Nat Neurosci. 2012; 15:1227–1235. [PubMed: 22820466]

Varela-Nallar L, Toledo EM, Larrondo LF, Cabral ALB, Martins VR, Inestrosa NC. Induction of cellular prion protein gene expression by copper in neurons. Am J Physiol, Cell Physiol. 2006; 290:C271–81. [PubMed: 16148034]

Voss J, Hubbell WL, Kaback HR. Helix packing in the lactose permease determined by metal-nitroxide interaction. Biochemistry. 1998; 37:211–216. [PubMed: 9425041]

Voss J, Hubbell WL, Kaback HR. Distance determination in proteins using designed metal ion binding sites and site-directed spin labeling: application to the lactose permease of Escherichia coli. Proc Natl Acad Sci USA. 1995a; 92:12300–12303. [PubMed: 8618889]

Voss J, Salwinski L, Kaback HR, Hubbell WL. A method for distance determination in proteins using a designed metal ion binding site and site-directed spin labeling: evaluation with T4 lysozyme. Proc Natl Acad Sci USA. 1995b; 92:12295–12299. [PubMed: 8618888]

Vranken WF, Boucher W, Stevens TJ, Fogh RH, Pajon A, Llinas M, Ulrich EL, Markley JL, Ionides J, Laue ED. The CCPN data model for NMR spectroscopy: Development of a software pipeline. Proteins. 2005; 59:687–696. [PubMed: 15815974]

Walter ED, Chattopadhyay M, Millhauser GL. The affinity of copper binding to the prion protein octarepeat domain: evidence for negative cooperativity. Biochemistry. 2006; 45:13083–13092. [PubMed: 17059225]

Walter ED, Stevens DJ, Spevacek AR, Visconte MP, Dei Rossi A, Millhauser GL. Copper binding extrinsic to the octarepeat region in the prion protein. Curr Protein Pept Sci. 2009; 10:529–535. [PubMed: 19538144]

Walter ED, Stevens DJ, Visconte MP, Millhauser GL. The prion protein is a combined zinc and copper binding protein: Zn2+ alters the distribution of Cu2+ coordination modes. J Am Chem Soc. 2007; 129:15440–15441. [PubMed: 18034490]

Wang L, Zhang Z, Brock A, Schultz PG. Addition of the keto functional group to the genetic code of Escherichia coli. Proc Natl Acad Sci USA. 2003; 100:56–61. [PubMed: 12518054]

Watt NT, Taylor DR, Kerrigan TL, Griffiths HH, Rushworth JV, Whitehouse IJ, Hooper NM. Prion protein facilitates uptake of zinc into neuronal cells. Nat Commun. 2012; 3:1134. [PubMed: 23072804]

Whittal RM, Ball HL, Cohen FE, Burlingame AL, Prusiner SB, Baldwin MA. Copper binding to octarepeat peptides of the prion protein monitored by mass spectrometry. Protein Sci. 2008; 9:332–343. [PubMed: 10716185]

Yang Z, Kise D, Saxena S. An approach towards the measurement of nanometer range distances based on Cu2+ ions and ESR. J Phys Chem B. 2010; 114:6165–6174. [PubMed: 20397677]

Yang Z, Kurpiewski MR, Ji M, Townsend JE, Mehta P, Jen-Jacobson L, Saxena S. ESR spectroscopy identifies inhibitory Cu2+ sites in a DNA-modifying enzyme to reveal determinants of catalytic specificity. Proc Natl Acad Sci USA. 2012; 109:E993–1000. [PubMed: 22493217]

You H, Tsutsui S, Hameed S, Kannanayakal TJ, Chen L, Xia P, Engbers JDT, Lipton SA, Stys PK, Zamponi GW. Aβ neurotoxicity depends on interactions between copper ions, prion protein, and N-methyl-D-aspartate receptors. Proc Natl Acad Sci USA. 2012; 109:1737–1742. [PubMed: 22307640]

Young TS, Ahmad I, Yin JA, Schultz PG. An enhanced system for unnatural amino acid mutagenesis in E. coli. J Mol Biol. 2010; 395:361–374. [PubMed: 19852970]

Highlights

- The N-terminal octarepeat domain of the prion protein takes up Cu^{2+}
- The octarepeat Cu^{2+} interacts with a negatively charged C-terminal domain pocket
- The C-terminal interaction surface overlaps the epitope of the toxic POM1 antibody
- POM1 may act by interfering with the Cu^{2+} promoted *cis* interaction

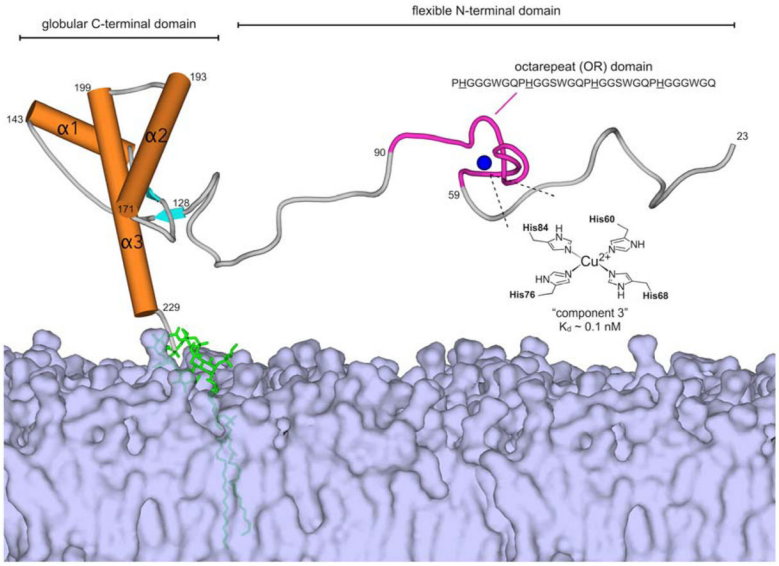

Figure 1. Structural Model of Membrane-anchored Mouse PrP^{C}

Three dimensional model of mouse PrP with numbers indicating key motifs and secondary structural elements. The globular C-terminal domain is defined by three α-helices (orange) and one short anti-parallel β-sheet (cyan) and is attached to the outer membrane by a C-terminal GPI ancher (green). The flexible N-terminal domain contains the octarepeat (OR) domain (magenta), which can coordinate Cu^{2+} in square planar geometry through the four OR histidines (inset).

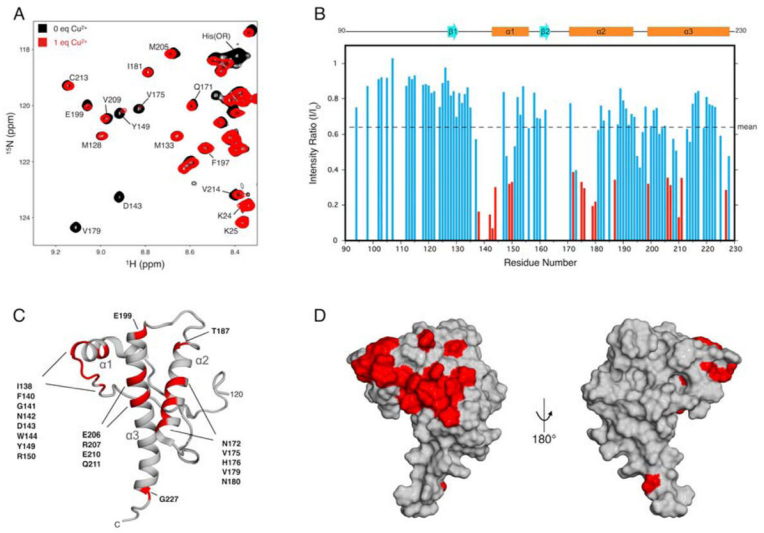

Figure 2. Cu^{2+}-binding Perturbs Specific Globular Domain Residues, Revealing the *cis* Interaction Surface

(A) Selected region of the ^{1}H-^{15}N HSQC NMR spectrum of MoPrP(H95Y/H110Y) in the absence of metal (black) and in the presence of 1 equivalent of Cu^{2+} (red) (see also Figure S2). (B) ^{1}H-^{15}N HSQC peak intensity reduction induced by Cu^{2+} for residues 90–230 of MoPrP(H95Y/H110Y). Intensity ratios for each residue are calculated as the peak height in the presence of 1 equivalent of Cu^{2+} over the peak height in the absence of metal. Residues displaying intensity reductions greater than one standard deviation are colored in red. Unassigned residues are omitted. (C) Globular domain residues significantly broadened by Cu^{2+}-binding are mapped onto the NMR structure of MoPrP(120–230, pdb 1xyx) and are colored red. (D) Surface plot of the MoPrP globular domain with the affected NMR resonances indicated in red.

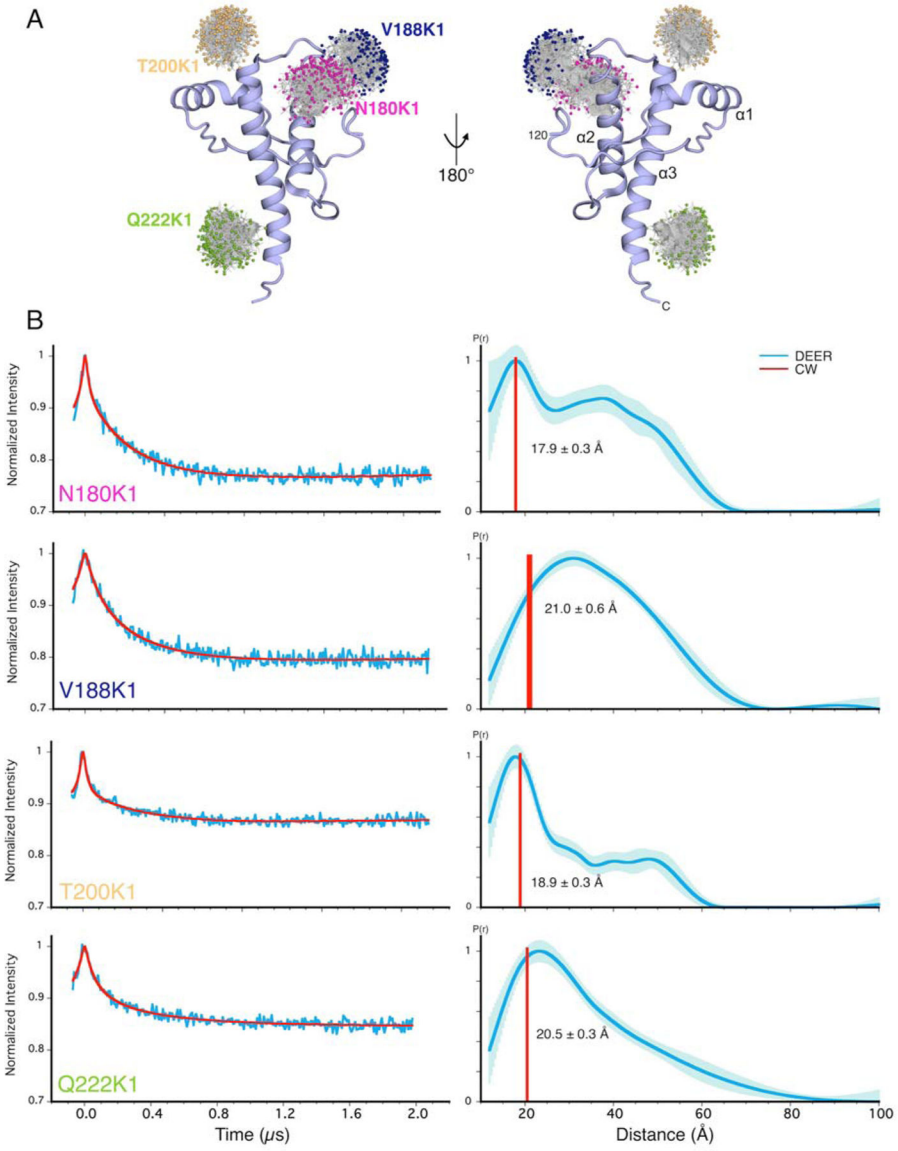

Figure 3. DEER Measurements Between Globular Domain Spin Labels and OR-bound Cu^{2+}

(A) Globular domain structure of MoPrP with predicted K1 spin label rotamers for each of the four spin-labeled constructs indicated in color. (B) Background-subtracted time-domain DEER data (left) and calculated distance distributions (right, blue trace) for spin-labeled variants of MoPrP(H95Y/H110Y) with 1 equivalent of Cu^{2+} at pH 6.0. Shaded areas on the distance distributions represent error estimations based on statistical perturbation of the signal noise and background subtraction. Vertical red bars indicate Cu^{2+}-nitroxide distances calculated from the room temperature CW amplitude reduction method with 1 equivalent Cu^{2+}, and bar widths correspond to the propagated error (±1 SD) based on three independent I/I_0 measurements (see also Figure 4).

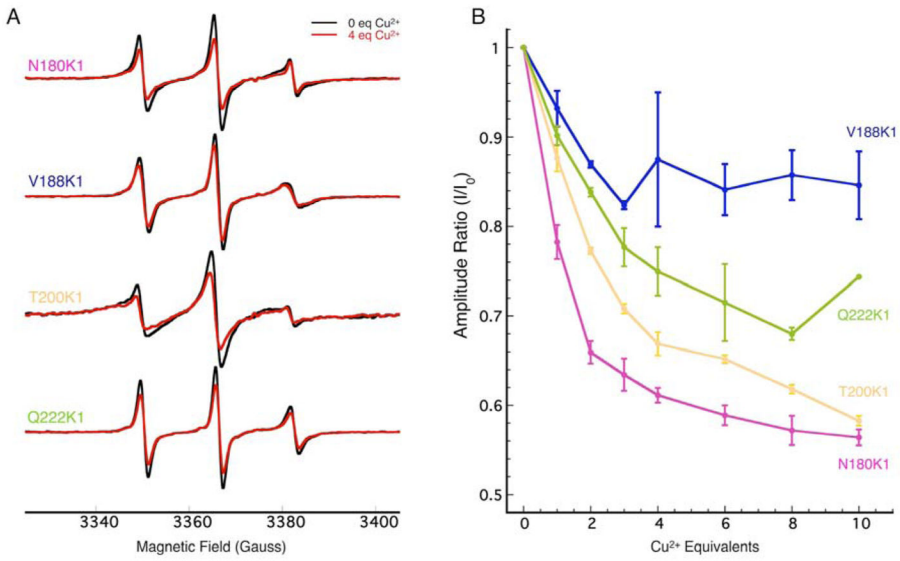

Figure 4. Distance-dependent Cu^{2+}-nitroxide Interactions in PrP from CW EPR Amplitude Reduction

(A) CW EPR spectra of K1 spin-labeled variants of MoPrP(H95Y/H110Y) at 298 K and pH 6.0 in the absence of metal (black) and in the presence of 4 equivalents of Cu^{2+} (red). (B) Peak-to-peak amplitude of the center ($m_I = 0$) line of the nitroxide EPR signal, relative to the amplitude of the metal-free spectrum, as a function of added Cu^{2+}. Error bars represent ±1 standard deviation based on three independent Cu^{2+} titrations.

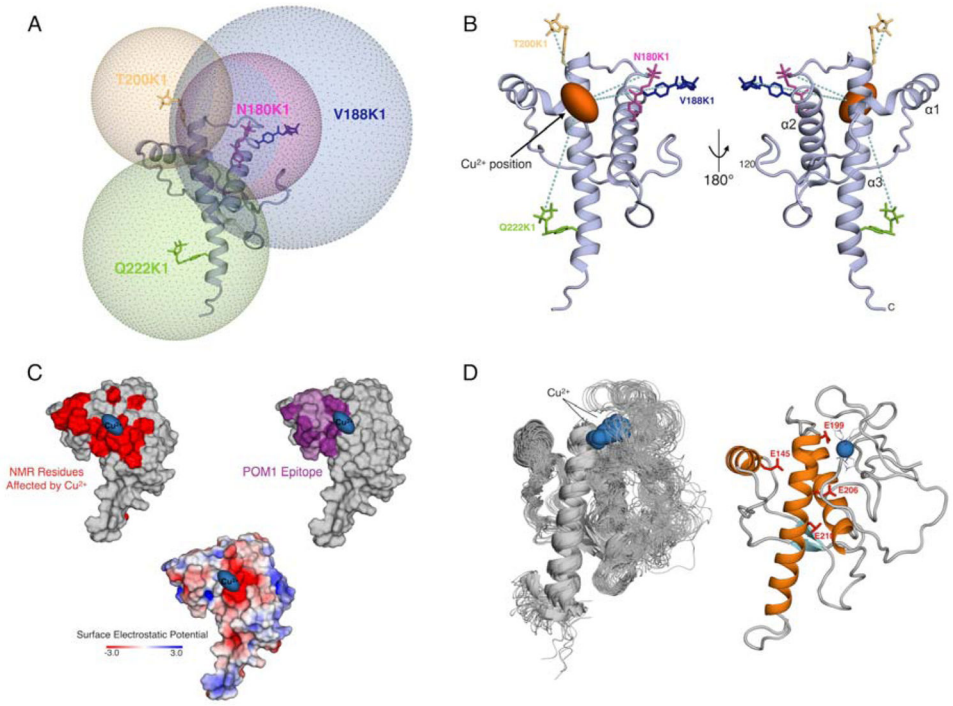

Figure 5. The OR-bound Cu^{2+} Ion is in Close Proximity to the POM1 Epitope and Coincides with a Charged Patch on the Globular Domain Surface

(A) Spin-labeled K1 rotamers modeled onto the PrP globular domain structure for use in Cu^{2+} trilateration. Spheres are centered at the unpaired electron of the nitroxide moiety with radii equal to the Cu-NO distances obtained from DEER EPR. (B) Results of the Cu^{2+} trilateration, assuming an arbitrary 5 Å standard deviation in each Cu^{2+}-K1 distance (see also Table S1). The calculated location (orange ellipsoid) places the Cu^{2+} ion at the exposed surface of helix 3. (C) Surface plots comparing the DEER-derived Cu^{2+} location (blue ellipsoid) with the residues affected by Cu^{2+}-binding in the ^{1}H-^{15}N HSQC NMR experiment (red), the conserved electronegative patch of the globular domain, and the POM1 epitope (purple). Residues that make direct contact with the POM1 $F(ab)_1$ fragment in the published crystal structure are colored dark purple. (D) Representative structures from MD trajectories of MoPrP(54–230), with Cu^{2+} bound as multi-His (component 3) in the N-terminal OR. Interdomain structure is stabilized by interaction between the OR-bound Cu^{2+} ion and acidic residues on helix 3.